Polymer Testing 161 (2026) 109298

Contents lists available at ScienceDirect

Polymer Testing

journal homepage: www.elsevier.com/locate/polytest

Effect of specimen geometry on the elastic characterization of particle-reinforced elastomers

Julen Cortazar-Noguerol *, Fernando Cortés, María Jesús Elejabarrieta

Department of Mechanics, Design and Industrial Management, University of Deusto, Avda. de las Universidades 24, Bilbao, 48007, Spain

ARTICLE INFO

Keywords:
Particle-reinforced elastomers
Shape factor
Particle concentration
Compression test
Torsion test
Poisson ratio

ABSTRACT

Compression- and torsion-based characterization of particle-reinforced elastomers yields geometry-dependent effective properties, limiting the reliability of material parameters used in engineering design and simulation. In this work, an experimental–modelling methodology is developed to estimate geometry-independent moduli under quasistatic and small-strain conditions. Cylindrical specimens covering a wide range of geometries and particle volume fractions are tested under compression and torsion conditions, providing the dataset for parameter identification. A phenomenological model combines particle reinforcement with geometry-dependent responses in both loading modes, showing that their interaction is not simply additive. The model is formulated to ensure simultaneous and physically consistent identification of elastic modulus, shear modulus, and Poisson's ratio. The model reproduces the measured effective properties with relative root-mean-square errors of approximately 7 % in compression, 6 % in shear and 11 % in Poisson's ratio. The resulting geometry-corrected moduli exhibit a linear increase with particle volume fraction, while Poisson's ratio slightly decreases due to stronger reinforcement in shear. A quantitative criterion is introduced to evaluate geometry-induced errors, establishing an admissible region based on a 10 % deviation threshold. The analysis shows that standard compression geometries can significantly overestimate the elastic modulus, whereas shear measurements remain more robust over a wider range of specimen shapes. For Poisson's ratio, the admissible limit lies outside practically achievable geometries. The methodology allows the estimation of moduli under quasistatic and small-strain conditions while providing practical guidelines for specimen design.

1. Introduction

Particle-reinforced elastomeric composites constitute an important class of engineering materials whose mechanical response can be tailored through composition. The elastomeric network provides large reversible deformation, while dispersed particles introduce additional load-transfer mechanisms and significantly enhance stiffness, strength, and wear resistance relative to the unfilled matrix [1,2]. These characteristics enable their widespread use in engineering sectors such as automotive and aerospace components and other structural applications [3].

Engineering implementation of composite materials requires accurate knowledge of their elastic properties [4–7]. In practice, elastic and shear moduli of soft composites are typically identified experimentally from uniaxial compression and shear or torsion tests [8–15], treating the measured response as representative of the material behavior. For elastomers this assumption is generally invalid because the measured mechanical response during testing depends strongly on boundary conditions and specimen geometry [16,17]. Classical rubber testing shows that in compression tests, bonding or friction between the specimen faces and the loading platens prevents lateral expansion, producing a confined deformation rather than uniaxial strain [8,16]. The degree of confinement is governed by the specimen geometry, with disk-like samples leading to increased effective compressive modulus [18–20]. Torsion measurements have shown an opposite effect: disk-like cylindrical specimens exhibit reduced effective shear stiffness relative to slender geometries, leading to incompatible moduli when geometry is not considered [21]. Consequently, the quantities obtained from standard experiments are geometry-dependent effective properties rather than material constants.

For isotropic materials the elastic and shear moduli are linked through Poisson's ratio. When the independently measured moduli are not strictly correlated, the inferred Poisson's ratio can take nonphysical values, frequently exceeding the incompressible limit of 0.5 [22].

* Corresponding author.
E-mail address: j.cortazar@deusto.es (J. Cortazar-Noguerol).

https://doi.org/10.1016/j.polymertesting.2026.109298
Received 20 April 2026; Received in revised form 9 July 2026; Accepted 13 July 2026
Available online 14 July 2026

In particle-reinforced elastomers the situation is further complicated by filler reinforcement. Rigid inclusions increase stiffness through load transfer and matrix constraint mechanisms [23–25], commonly described by classical reinforcement relations such as the Guth-Gold model. Experimental studies report stiffness increases with particle concentration under both compression and shear loading [26–29]. When filler reinforcement and specimen geometry effects are present, reinforcement modifies the internal stress distribution while specimen geometry controls the boundary constraints acting on that distribution. Consequently, the measured moduli may contain coupled contributions from filler addition and geometric confinement. These two phenomena have been examined separately in the literature but their combined influence on the experimentally determined elastic constants has not been investigated.

In previous studies by the authors, this geometry-induced bias was experimentally quantified and modeled in unfilled elastomers under both quasistatic and dynamic conditions, enabling geometry-independent elastic properties to be obtained from compression and torsion measurements [16,17]. The present work extends the developed framework to the quasistatic testing of particle-reinforced elastomeric composites through a combined experimental and modelling approach based on geometry-dependent measurements. Cylindrical specimens with varying shape factors and particle volume fractions are tested under matched quasistatic compression and torsion conditions. Geometry-dependent relations are incorporated into a phenomenological formulation previously applied to the unfilled matrix, whose parameters evolve with particle concentration. The analysis shows that particle reinforcement and specimen geometry cannot be treated as independent contributions: the presence of particles modifies the dependence of the effective properties on the shape factor. Simultaneous fitting of both tests enables the estimation of the elastic modulus, shear modulus, and Poisson's ratio under the selected quasistatic and small-strain conditions as functions of filler volume fraction.

The paper is organized as follows. Section 2 introduces the theoretical framework, including the influence of specimen geometry and filler reinforcement. Section 3 describes the materials and experimental procedures, and Section 4 presents the experimental results. Section 5 describes the phenomenological model and shows the parameter identification procedure. Section 6 introduces a quantitative criterion to evaluate geometry-induced errors and establishes practical limits for specimen design. Finally, Section 7 summarizes the main conclusions.

2. Theoretical framework

This section introduces the theoretical background required for this work. Linear elasticity relations relevant to compression and torsion tests are first shown, followed by a description of the influence of sample geometry on the measured elastic properties. Finally, a well stablished model of filler reinforcement in elastomers is described to account for the effect of particle volume fraction on the mechanical response of the composite material.

2.1. Elastic properties

The specimens used in this study are cylindrical, and the tests were performed under small-strain conditions. Therefore, the measured axial and torsional responses were analyzed using the classical linear-elastic relations for compression and torsion of circular cylinders.

In compression, the load F applied along the cylinder axis produces an axial displacement δ (see Fig. 1 (a)). Under quasistatic conditions and assuming a linear regime, these quantities are related by [8]

$$F = \frac{EA}{L}\delta \tag{1}$$

where E is the elastic modulus of the tested material, and $A = \pi d^2/4$ is the cross-sectional area for a cylindrical sample of diameter d and length L.

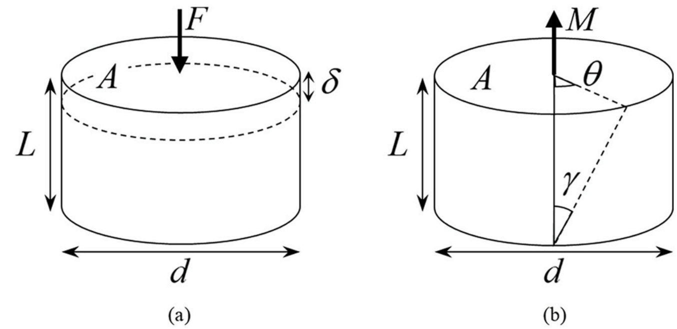

Fig. 1. Deformation modes in cylindrical specimens during (a) compression and (b) torsion tests.

Torsion tests on cylindrical specimens are characterized by an applied torque M and the corresponding twist angle θ (see Fig. 1 (b)). For small deformations and within linear elasticity, the torque–twist relationship for a solid cylinder is given by

$$M = \frac{GI_0}{L}\theta \tag{2}$$

where G denotes the shear modulus and $I_0 = \pi d^4/32$ is the polar moment of inertia of the circular cross section. The shear stress at the outer radius of the cylinder is $\tau = Md/2I_0$ and its associated shear strain is $\gamma = d\theta/2L$.

The axial and shear responses are connected in isotropic materials through Poisson's ratio ν, which yields the relationship

$$\nu = \frac{E}{2G} - 1 \tag{3}$$

Consequently, independent measurements of E and G obtained from compression and torsion tests allow ν to be determined through Eq. (3). Under the same assumption, the bulk modulus K can also be obtained from E and G as

$$K = \frac{EG}{3(3G - E)} \tag{4}$$

For incompressible or near incompressible materials, the volume remains almost constant during deformation, it follows that $\nu \approx 0.5$ and $E \approx 3G$. Therefore, the denominator in Eq. (4) tends to zero and $K \to \infty$.

2.2. Effect of the sample shape on the measured properties

The measured effective properties of cylindrical specimens are influenced by the geometry of the sample. In axial compression, the measured properties are influenced by the lateral confinement imposed by the contact surfaces [18]. This effect can be described through the shape factor S of the sample, defined as the ratio between the loaded area and the free-to-bulge area as

$$S = \frac{A_{\text{load}}}{A_{\text{free}}} = \frac{\pi d^2/4}{\pi dL} = \frac{d}{4L} \tag{5}$$

Large values of S correspond to wide disk-like specimens that experience strong lateral constraint, which artificially increases the measured effective compressive modulus E_S of the sample. This behavior is well established for elastomers and is commonly described through the expression [8,19]

$$E_S(S) = E(1 + \beta S^n) \tag{6}$$

where E is the elastic modulus of the tested material, and β and n govern the rate at which geometric confinement increases the effective modulus. As $S \to 0$, corresponding to rod-like specimens, E_S converges to the material modulus E. This trend was previously validated experimentally in silicone rubber across a broad range of geometries [16].

Torsional measurements are also sensitive to geometry, although the mechanisms differ from those of compression. High S specimens tend to exhibit lower effective shear modulus G_S while long, slender samples (low S) produce more reliable and geometry-independent shear responses. The absence of an existing correction model analogous to the compressive case motivated the introduction of a phenomenological model describing this dependency [16]. The proposed expression for the effective shear modulus is

$$G_S(S) = G\frac{1+\beta S^n}{1+\alpha S^n} \tag{7}$$

where G is the shear modulus of the material, the parameters β and n are shared with the compressive model and α is an added parameter which governs the extent of the effective shear modulus decrease. This behavior was confirmed in the previous study, which showed a reduction of G_S with increasing S.

Substituting the expressions for $E_S(S)$ and $G_S(S)$ in Eq. (3) yields the corresponding effective Poisson's ratio:

$$\nu_S(S) = \nu + \frac{E}{2G}\alpha S^n \tag{8}$$

where ν is the Poisson's ratio of the material as defined in Eq. (3). This formulation reproduces the strong growth of the effective Poisson's ratio with increasing S observed experimentally and explains why uncorrected measurements frequently exceed the incompressible limit of 0.5 in isotropic elastomers.

Together, the models in Eqs. (6)–(8) enable quantification and correction of specimen geometry effects in compression and torsion tests.

2.3. Filler reinforcement in elastomers

The addition of rigid particulate fillers into an elastomeric matrix modifies the elastic response of the material through load transfer and matrix constraint mechanisms. For isotropic composites containing spherical inclusions, classical homogenization approaches establish an increase in both elastic and shear moduli with increasing volume fraction of the filler [23].

Assuming small deformations and dilute to moderate filler concentrations, typically lower than 30 % volume fraction, the reinforcement effect is often described by expressing the modulus of the composite as a function of filler volume fraction φ. A general representation can be written in polynomial form as [30]

$$M(\varphi) = M_0\left(1 + a_1\varphi + a_2\varphi^2 + \ldots + a_p\varphi^p\right) \tag{9}$$

where $M = \{E, G\}$ represents the elastic or shear modulus, M_0 is the modulus of the unfilled matrix and a_i are the material-dependent coefficients accounting for particle stiffness, particle-matrix interactions and inter-particle effects. For perfectly spherical rigid particles, an ideally incompressible matrix and accounting for the interaction between pairs of particles, Guth & Gold proposed the well-known second-order expression [23,30]:

$$M(\varphi) = M_0\left(1 + 2.5\varphi + 14.1\varphi^2\right) \tag{10}$$

3. Materials and methods

This section outlines the preparation of the composite samples, the equipment and the experimental methods employed.

3.1. Sample preparation

The composite material studied was prepared by mixing a silicone rubber matrix with rigid ferromagnetic particles. On the one hand, the matrix of the composite was a commercially available room temperature vulcanization (RTV) silicone rubber supplied by WACKER, known as ELASTOSIL® M 4644 A/B [31]. This two-component silicone rubber vulcanizes at room temperature when its two components (A and B) are mixed in a 10:1 wt ratio. According to the technical sheet provided by the supplier, the resultant density of the matrix is $\rho_{\mathrm{M}} = 1.07\ \mathrm{g/cm^3}$, where the M subindex stands for 'matrix'.

On the other hand, the ferromagnetic material embedded in the matrix were spherical carbonyl-iron powder (CIP) particles supplied by BASF. According to the supplier, these particles have $1.25 \pm 0.55\ \mu\mathrm{m}$ average diameter and their density is $\rho_{\mathrm{CIP}} = 7.8\ \mathrm{g/cm^3}$.

Samples with four different CIP volume fractions (φ_{CIP}) under the moderate concentration threshold were prepared: 5 %, 10 %, 15 % and 20 %. To achieve a wide range of sample geometries, molds were fabricated from polymethyl methacrylate (PMMA) sheets of two thicknesses (3 and 10 mm) using a ROLAND MDX-40A [32] 3D milling machine (see Fig. 2 (a)). Each mold contains cylindrical holes with diameters of 5, 10, 15, and 20 mm (Fig. 2 (b)). This combination of sheet thicknesses and hole diameters yields 8 distinct nominal sample sizes, from which 7 were selected to ensure an approximately uniform coverage of the shape factor range. The 5 mm diameter and 3 mm thickness specimens were excluded due to handling difficulties and because their shape factor lies within that defined by the 10 mm thick specimens with 15 mm and 20 mm diameters.

To obtain the different volume fractions of CIP the needed mass can be obtained as a function of known parameters as

$$m_{\mathrm{CIP}} = \frac{\varphi_{\mathrm{CIP}}}{1-\varphi_{\mathrm{CIP}}}\frac{\rho_{\mathrm{CIP}}}{\rho_{\mathrm{M}}}m_{\mathrm{M}} \tag{11}$$

where m_{M} is the total mass of the silicone rubber matrix.

Component A is first weighted in a precision balance. CIP is then added in the required mass, calculated using Eq. (11) to obtain the desired particle volume fraction, and the mixture is manually stirred. Subsequently, component B is incorporated in a 10:1 (A:B) weight ratio. The resulting composite is poured into cylindrical molds within 30 min after mixing. Vacuum cycles are applied at each step to remove any air bubbles present using a vacuum chamber (Fig. 2 (c)). The molds are then sealed and left to cure for 24 h before demolding. For each nominal geometry, 3 specimens are prepared, yielding 21 samples per particle volume fraction. In Fig. 2 (d) a set of samples of a single concentration and different shape factors is shown.

3.2. Experimental equipment

This subsection describes the experimental equipment used for the characterization of the prepared composite samples.

On the one hand, to measure the effective compressive modulus, quasistatic strain ramps are performed using a Dynamic Mechanical Analyzer (DMA) equipped with a compression clamp, specifically, the DMA Q800 model fabricated by T.A. Instruments (Fig. 3 (a)). This equipment can generate force-controlled displacements with a range from 0.001 N to 18 N and measure displacements with 1 nm resolution. The data acquisition is done using Advantage for Q Series Version 2.9.2.396 software, provided by T.A. Instruments and the subsequent processing and analysis are carried out in MATLAB R2025a.

On the other hand, to measure the effective shear modulus, quasistatic shear strain ramps are performed using the Anton Paar Modular Compact Rheometer (MCR) 302e with a parallel plate configuration (Fig. 3 (b)). This rheometer can exert axial compressive forces up to 50 N and 230 mN m maximum torque and measure angular displacements with a resolution of 0.05 μrad. Data acquisition is performed through RheoCompass v1.33.491, and the subsequent processing and analysis are carried out in MATLAB R2025a.

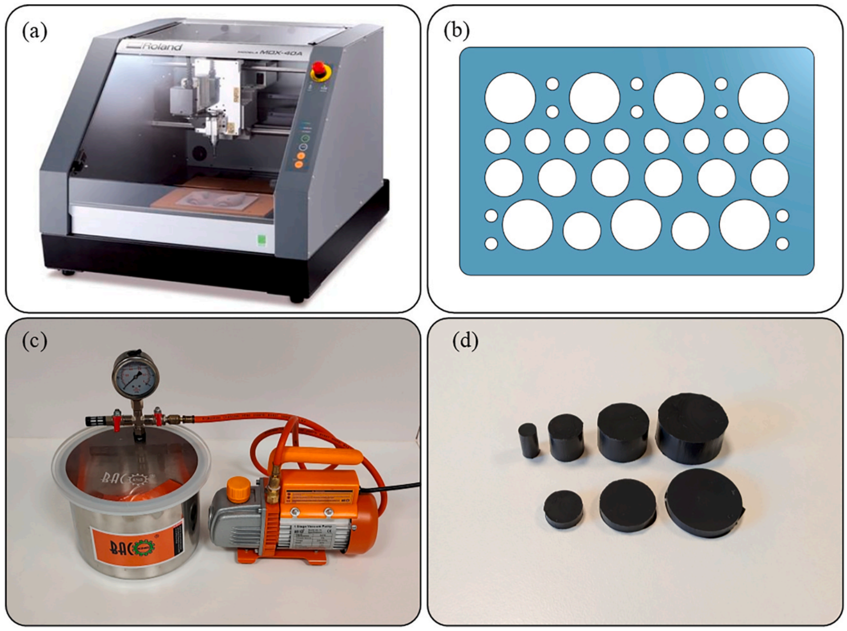

Fig. 2. Equipment and materials used for the preparation of particle-reinforced elastomer samples: (a) ROLAND MDX-40A 3D milling machine; (b) cylindrical mold made of PMMA; (c) vacuum chamber and pump and (d) composite samples of various sizes.

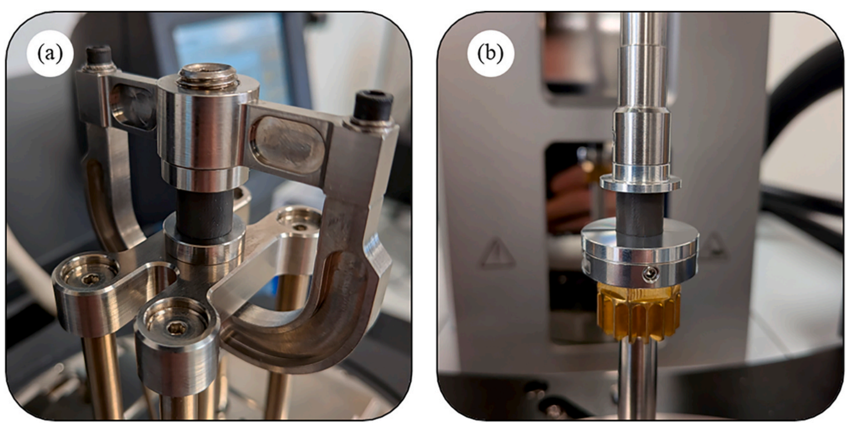

Fig. 3. Experimental equipment used for characterization: (a) DMA equipped with a compression clamp and (b) rheometer with a parallel-plate configuration.

3.3. Experimental methods

To obtain the compressive and shear moduli of cylindrical composite samples with different CIP volume fractions, 3 specimens are tested for each of the 7 nominal geometries to ensure repeatability, giving a total of 21 measurements per concentration. Correlating the effective moduli and deriving the effective Poisson's ratio requires that compression and torsion tests be carried out under equivalent conditions, including strain rate, axial pre-strain, and temperature. This approach is consistent with the intent behind Tschoegl's protocol [33]. While that protocol prescribes simultaneous measurements on a single device, the present work employs separate testing setups operated under rigorously aligned conditions.

Quasistatic strain ramps are conducted in the DMA (compression) and the rheometer (torsion) to obtain effective compressive and shear moduli respectively. Preliminary tests were performed to ensure strain-rate and pre-strain independence of the results in both the compression and torsion tests as well as linear behavior up to the maximum strain. The selected strain-rate is 0.2 %/min and the maximum strain is 1 % in both cases. All tests are conducted at room temperature (25± 2 °C). Because the silicone rubber matrix lies in the viscoelastic rubbery regime, far from transition (reported to be bellow −60 °C [14]), small temperature variations within this range are not expected to affect the measured moduli.

A small axial pre-strain was required in torsion to prevent slipping at the sample–plate interfaces. Although such pre-strain is not necessary for quasistatic compression, identical conditions were imposed in both setups to ensure consistency between the measurements. The DMA operates in force-controlled mode. Therefore, the force required to achieve the selected pre-strain for each geometry was determined from previously established quasistatic relations between shape factor and effective compressive modulus [16]. An axial pre-strain of $\varepsilon_0 = 0.5$ % was adopted for both test configurations ensuring it was sufficiently small to avoid affecting the compression measurements and sufficiently large to prevent wall slip in torsion tests.

4. Experimental results

This section presents the experimental results obtained from the compression and torsion tests. For each nominal geometry, 3 specimens are tested to ensure repeatability. The reported values correspond to the slopes of linear regressions of the measured stress–strain curves, shown as the mean value and standard deviation for each nominal size and particle volume fraction.

4.1. Effect of shape factor on the effective moduli

The effect of the sample shape factor on the effective moduli is evaluated by representing them as a function of shape factor for the different particle volume fractions tested.

Fig. 4(a) and (b) presents the effective compressive modulus E_S and the effective shear modulus G_S as a function of the sample shape factor S for all investigated CIP volume fractions (represented as different markers and colors).

On the one hand, a clear increase in E_S with increasing S is observed for all concentrations, reflecting the progressive stiffening induced by lateral confinement in cylindrical specimens. This trend is consistent with the well-established influence of geometric constraint in elastomer compression tests [16]. Measurements for the highest filler content (20 %) and shape factor (1.67) could not be obtained as the required compressive force exceeded the operational limit of the DMA. Operating close to the force limit of the instrument also led to increased experimental uncertainty, as reflected by the larger dispersion bars observed in the measured values of higher S.

On the other hand, G_S exhibits a decreasing trend with increasing S for all concentrations, indicating a progressive reduction of the measured shear stiffness in short, disk-like specimens. This trend is consistent with the previous results obtained when testing the elastomeric matrix [16].

The experimental scatter between samples with the same nominal dimensions remains limited across most geometries and compositions, only standard deviations greater than 5 % have been represented in Fig. 4. This level of dispersion confirms the good repeatability of both the sample preparation and the experimental measurements.

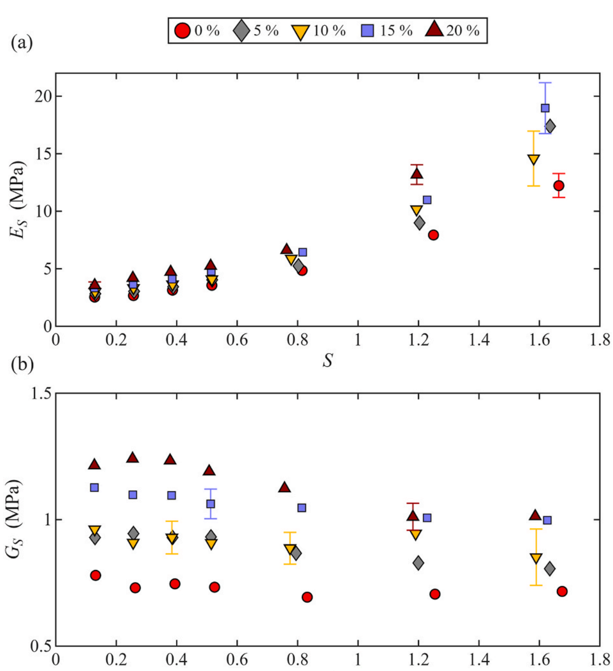

Fig. 4. Effective (a) compressive modulus and (b) shear modulus as functions of shape factor for composites with different CIP volume fractions. Each marker represents the mean value from three nominally identical samples, and the vertical bars denote the corresponding standard deviations (only standard deviations >5 % are shown).

4.2. Effect of particle volume fraction on the effective moduli

The effect of filler volume fraction on the measured mechanical response is examined by analyzing the effective moduli at fixed sample geometry. Figs. 5 and 6 present the effective compressive modulus E_S and the effective shear modulus G_S, respectively, as functions of the CIP volume fraction for each nominal shape factor.

For a given shape factor, both E_S and G_S increase with filler volume fraction. Over the investigated concentration range, this dependence is well approximated by a linear relation for all geometries. Linear fits are included for reference in dashed grey lines.

5. Modelling and parameter identification

This section introduces a phenomenological model to describe the combined influence of sample geometry and particle volume fraction on the effective mechanical response. The model parameters are determined through curve fitting to the experimental data. The composite material's elastic properties can then be extracted as functions of the particle volume fraction, independent of sample geometry.

5.1. Model formulation including filler reinforcement and shape factor effects

Based on the observations in Section 4, a phenomenological model is formulated to describe the effective compressive and shear moduli as functions of specimen geometry and particle volume fraction. The geometry-dependent relations introduced in Section 2.2 are retained, and, based on the approximately linear dependence on particle volume fraction observed in Section 4, only the linear term of Eq. (9) is considered to represent filler reinforcement. In addition, the shape factor effect is modeled following Eqs. (6) and (7), and the parameters $\beta = \beta_0(1 + k_\beta\varphi)$ and $\alpha = \alpha_0(1 + k_\alpha\varphi)$ are allowed to depend linearly on the particle volume fraction. The resulting expressions for the effective compressive and shear moduli are written as

$$E_S(S,\varphi) = E_0(1 + k_E\varphi)\left[1 + \beta_0(1 + k_\beta\varphi)S^n\right] \tag{12}$$

$$G_S(S,\varphi) = G_0(1 + k_G\varphi)\frac{1 + \beta_0(1 + k_\beta\varphi)S^n}{1 + \alpha_0(1 + k_\alpha\varphi)S^n} \tag{13}$$

Here, $E_0 = E_S(S\to 0, \varphi = 0)$ and $G_0 = G_S(S \to 0, \varphi = 0)$ represent the elastic and shear moduli of the unfilled silicone rubber matrix, obtained in the limit of vanishing shape factor, and β_0, α_0 and n are the model parameters for the silicone rubber matrix [16]. The coefficients k_E and k_G represent the proportionality constants for filler reinforcement of the composite material while k_β and k_α quantify how this filler reinforcement modify the shape factor dependence of the effective moduli.

To obtain an expression consistent with the approximately linear reinforcement behavior observed experimentally (Section 4.2), Eqs. (12) and (13) are expanded about $\varphi = 0$ using their Taylor series and truncated at first order. This expansion yields the following approximations for the effective compressive and shear moduli:

$$E_S = E_0(1 + \beta_0 S^n)\left[1 + \left(k_E + \frac{\beta_0 k_\beta S^n}{1 + \beta_0 S^n}\right)\varphi\right] \tag{14}$$

$$G_S = G_0\frac{1 + \beta_0 S^n}{1 + \alpha_0 S^n}\left[1 + \left(k_G + \frac{\beta_0 k_\beta S^n}{1 + \beta_0 S^n} - \frac{\alpha_0 k_\alpha S^n}{1 + \alpha_0 S^n}\right)\varphi\right] \tag{15}$$

Eqs. (14) and (15) are linear in particle volume fraction while preserving the shape-factor dependence of the geometry correction, and are therefore used for parameter identification in the following section.

5.2. Parameter identification via curve fitting

The parameters E_0, G_0, β_0, α_0 and n are taken from the previously

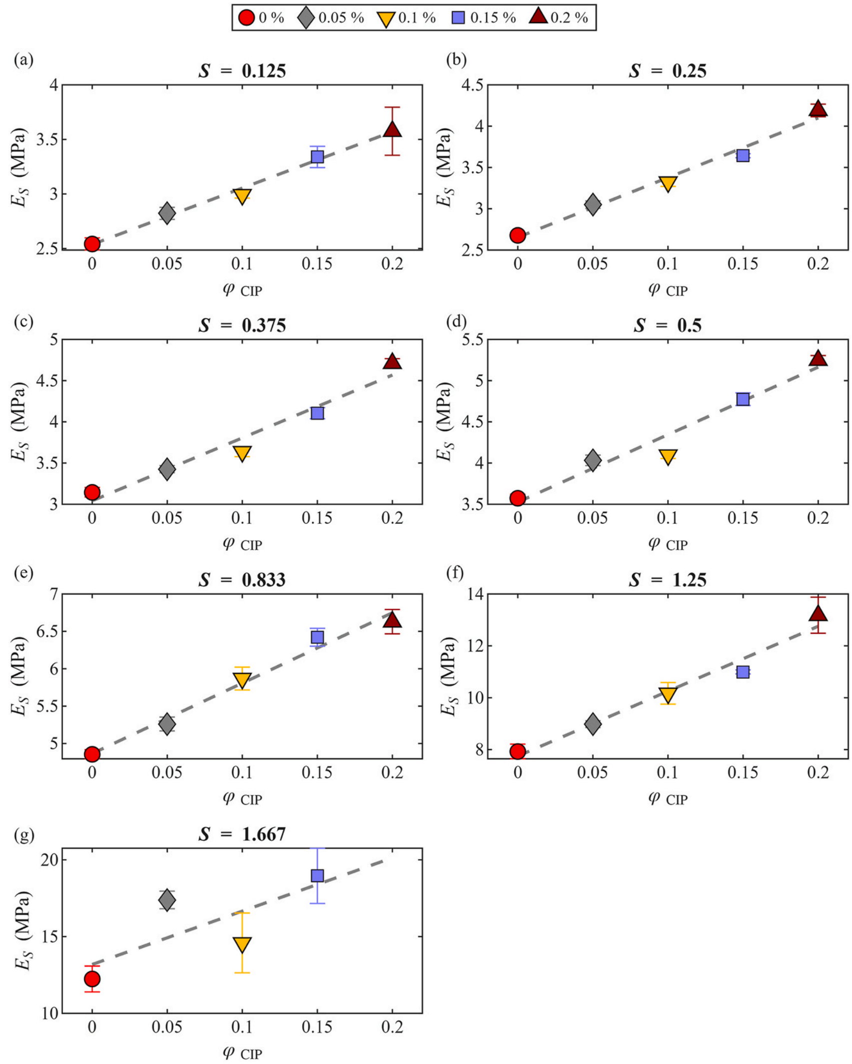

Fig. 5. Effective compressive modulus as a function of filler volume fraction. A linear regression of the experimental data is represented by a dashed grey line. (a) to (g) represent the different nominal shape factor tested.

characterized unfilled silicone rubber matrix and are kept fixed during the identification procedure. These parameters define the reference response of the matrix material, and fixing them avoids re-identifying the matrix behavior from the composite data, thereby reducing the number of fitted variables and improving the robustness of the optimization. Their numerical values are summarized in Table 1. Parameters k_E, k_G, k_β and k_α are determined by curve fitting of the present experimental data.

To determine the value of each presented parameter, the function 'fmincon' of MATLAB R2025a is used. The parameter estimation problem is formulated as a nonlinear constrained optimization and solved using an interior-point algorithm. Constraint enforcement is achieved through a barrier approach, while search directions are computed via approximate solutions of the Karush–Kuhn–Tucker system using quasi-Newton Hessian updates combined with a line-search globalization strategy [34]. High limits on function evaluations and iterations were imposed to prevent premature termination, while strict tolerances on objective reduction and step norm were enforced to avoid convergence to flat or ill-conditioned regions.

The model parameters are identified by minimizing the difference between the experimental measurements and the predictions of Eqs. (14) and (15). For each specimen geometry and particle volume fraction, residuals are defined as the difference between the measured and predicted effective moduli. The objective function is constructed as the sum of the squared normalized residuals for both compression and shear tests,

$$\mathscr{J}(\mathbf{X}) = \sum_{i,j}\left[\left(\frac{E^{\mathrm{exp}}_{i,j} - E_S(S_i,\varphi_j,\mathbf{X})}{E^{\mathrm{exp}}_{i,j}}\right)^2 + \left(\frac{G^{\mathrm{exp}}_{i,j} - G_S(S_i,\varphi_j,\mathbf{X})}{G^{\mathrm{exp}}_{i,j}}\right)^2\right] \quad (16)$$

where $E^{\mathrm{exp}}_{i,j}$ and $G^{\mathrm{exp}}_{i,j}$ are the experimental values of the effective compressive and shear moduli for the sample with shape factor S_i and volume fraction φ_j and $\mathbf{X} = \{k_E, k_G, k_\beta, k_\alpha\}$ is the vector of fitted parameters. Normalization by the measured moduli prevents bias towards the data with larger absolute magnitude and allows both test types to contribute comparably to the identification of parameters.

Optimization includes physically motivated nonlinear constraints to ensure mechanical admissibility of the identified properties. Over the investigated concentration range, the Poisson's ratio is required to decrease with particle volume fraction, while the corresponding bulk modulus must increase, as reported in the literature [35,36]. The parameter vector is therefore obtained by minimizing Eq. (17) subject to these conditions, so that only parameter sets consistent with the expected behavior of particle-reinforced elastomers are accepted.

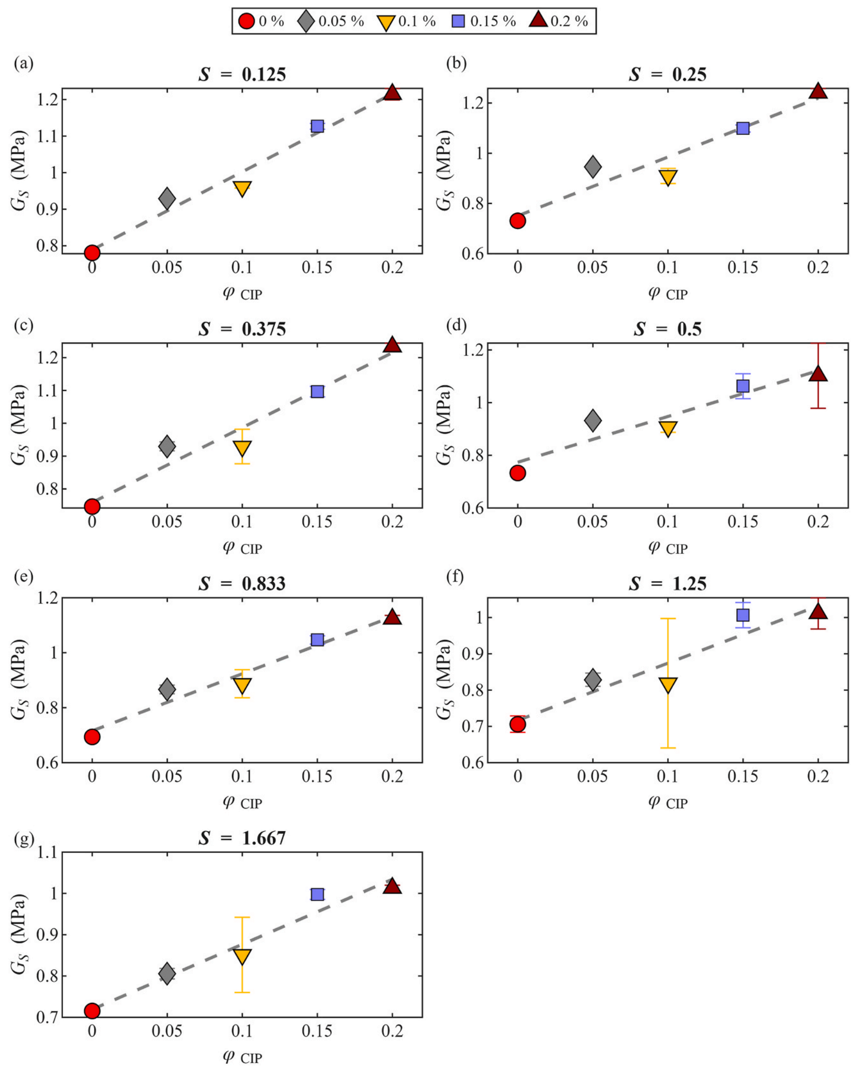

Fig. 6. Effective shear modulus as a function of filler volume fraction. A linear regression of the experimental data is represented by a dashed grey line. (a) to (g) represent the different nominal shape factor tested.

Table 1
Values of the obtained parameters for the shape factor correction of the unfilled silicone rubber [16].

E_0	G_0	β_0	α_0	n
2.26 MPa	0.763 MPa	1.75	2.01	1.85

5.3. Parameters and model validation

The model parameters were identified using the optimization procedure described in Section 5.2 through simultaneous fitting of the compression and torsion data. The identified values of the reinforcement and geometry-modification coefficients are summarized in Table 2.

The identified coefficients provide information on how particle addition affects both the elastic response and the geometry-dependent contribution. The fact that k_G is slightly bigger than k_E implies that the shear modulus increases more rapidly with particle volume fraction than the elastic modulus, which results in a small decrease of the Poisson's ratio with filler content. Moreover, the obtained values for k_E and k_G are close to those proposed by Guth & Gold [30] (Eq. (10)). The negative value of k_β indicates that particle addition slightly reduces the shape-factor contribution in compression, leading to a less pronounced increase of the effective compressive modulus. Given k_α is also negative and $|k_\alpha| > |k_\beta|$, the particle addition increases the shape factor effect in the effective shear modulus measured in torsion tests.

Table 2
Identified parameter values.

k_E	k_G	k_β	k_α
2.71	2.74	−0.159	−0.314

Additionally, the slope of the moduli with respect to particle volume fraction $k_M^{\text{eff}}(S) = \partial M_S(S,\varphi)/\partial\varphi$, is shown as a function of shape factor in Fig. 7. The compressive slope decreases with shape factor, whereas the shear slope increases. Consequently, specimens with larger shape factors exhibit a stronger apparent reinforcement in torsion but a weaker apparent reinforcement in compression.

For model validation, Fig. 8 compares the model predictions with the experimental measurements of the effective compressive and shear moduli as functions of shape factor for all investigated particle volume fractions. The continuous curves correspond to the values obtained from Eqs. (14) and (15) using the parameters listed in Table 2, while the symbols represent the experimental data. The model reproduces the increase of the effective compressive modulus with shape factor as well as the progressive decrease of the effective shear modulus, capturing also the dependence on the filler reinforcement volume fraction. The

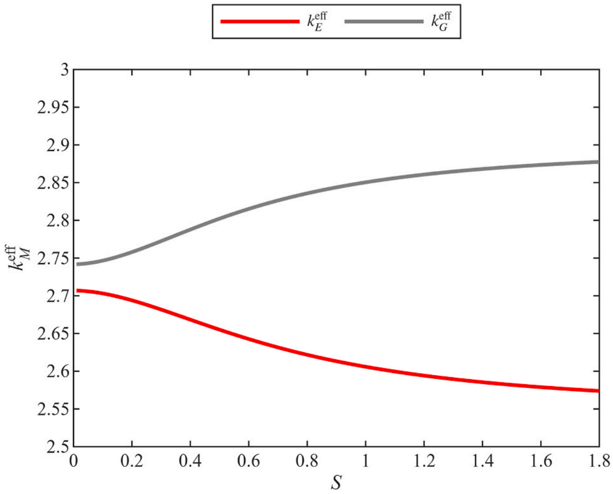

Fig. 7. Reinforcement slopes with respect to particle volume fraction as functions of shape factor predicted by the model for the effective compressive and shear moduli.

agreement is maintained over most of the investigated geometries and concentrations, although the deviations become slightly larger at higher particle volume fractions, particularly for increasing shape factor.

To quantify the accuracy of the identified model, the relative root-mean-square error (RRMSE) is evaluated for the effective compressive modulus, the effective shear modulus, and the derived Poisson's ratio. The metric is computed separately for each particle volume fraction by comparing the model predictions with the corresponding experimental measurements. For a generic measured data M, the RRMSE is defined as

$$\text{RRMSE}(M) = \sqrt{\frac{1}{N}\sum_{i=1}^{N}\left(\frac{M_i^{\text{model}} - M_i^{\text{exp}}}{M_i^{\text{exp}}}\right)^2} \tag{17}$$

where M_i^{model} and M_i^{exp} represent the model predicted and the experimental values, respectively and N is the number of measurements considered. Applying this definition to both moduli it is obtained that $\text{RRMSE}(E_S) = 0.07$ and $\text{RRMSE}(G_S) = 0.06$, and for the Poisson's ratio predictions $\text{RRMSE}(\nu_S) = 0.11$.

The obtained errors indicate good agreement between the model predictions and the experimental measurements. The RRMSE values of 7 % for the effective compressive modulus and 6 % for the effective shear modulus are of the same order as the experimental scatter observed in the experimental data. This suggests that the remaining differences are primarily associated with measurement scatter and specimen-to-specimen variability rather than deficiencies of the model. Therefore, the RRMSE was retained as a conservative error estimate for the subsequent interpretation of the geometry-independent properties identified from the model.

5.4. *Quasistatic small-strain elastic properties as functions of particle volume fraction*

The identified model allows the elastic properties of the composite to be determined independently of specimen geometry under the current experimental conditions. In the present framework, the elastic properties correspond to the limit of $S \to 0$ in Eqs. (14) and (15), for which the geometry-induced correction disappears and the measured moduli reduce to material parameters defined by

$$E = E_0(1 + k_E\varphi) \tag{18}$$

$$G = G_0(1 + k_G\varphi) \tag{19}$$

$$\nu = \frac{E}{2G} - 1 = \frac{(\nu_0 + 1)(1 + k_E\varphi)}{(1 + k_G\varphi)} - 1 = \frac{\nu_0(1 + k_E\varphi) + (k_E - k_G)\varphi}{(1 + k_G\varphi)} \tag{20}$$

where $\nu_0 = E_0/(2G_0) - 1$ is the Poisson's ratio of the unfilled silicone rubber matrix. Based on the results presented in Section 5.3, Fig. 9 shows the estimated elastic properties of the composite as a function of filler volume fraction. Here, the solid lines represent Eqs. (18)–(20), and the shaded region represents the RRMSE associated with the model prediction for each particle volume fraction.

Both moduli increase linearly with particle volume fraction, indicating a consistent reinforcement of the elastomer matrix due to particle addition. In contrast, Poisson's ratio exhibits a slight decrease, from 0.481 to 0.474, due to the stronger increase of the shear modulus relative to the elastic modulus. However, this variation is lower than the estimated RRMSE of the model and should therefore be interpreted as a weak trend, although it is consistent with previously reported behavior in filled polymer composites [35–37]. These results indicate that accounting for geometry effects can improve the estimation of elastic properties in particle-reinforced elastomers from compression and torsion measurements, providing more reliable parameters for small-strain elastic modelling and composite material design and resulting in physically feasible values for Poisson's ratio.

6. Quantification of geometry-induced errors

This section introduces a quantitative criterion to evaluate the influence of specimen geometry on the measured elastic properties. A tolerance of 10 % is adopted, consistent with the predictive accuracy of the identified model. The relative deviation between the effective modulus at a given shape factor and the corresponding material property is defined as

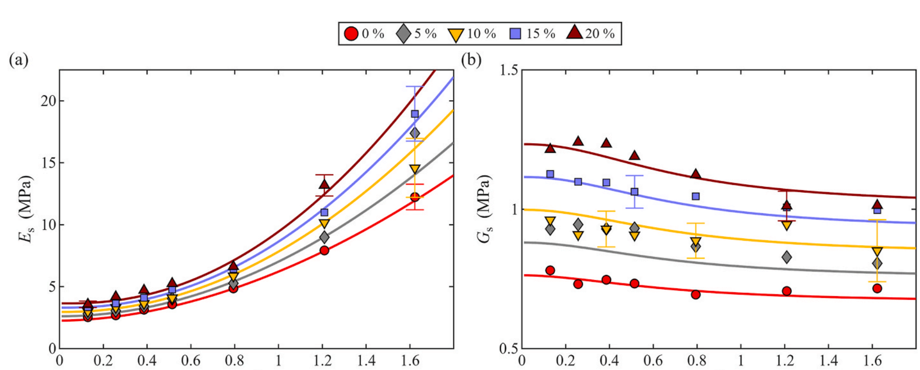

Fig. 8. Effective moduli as a function of the shape factor for different particle volume fractions: (a) effective compressive modulus and (b) effective shear modulus. Symbols represent experimental measurements and solid lines the model predictions.

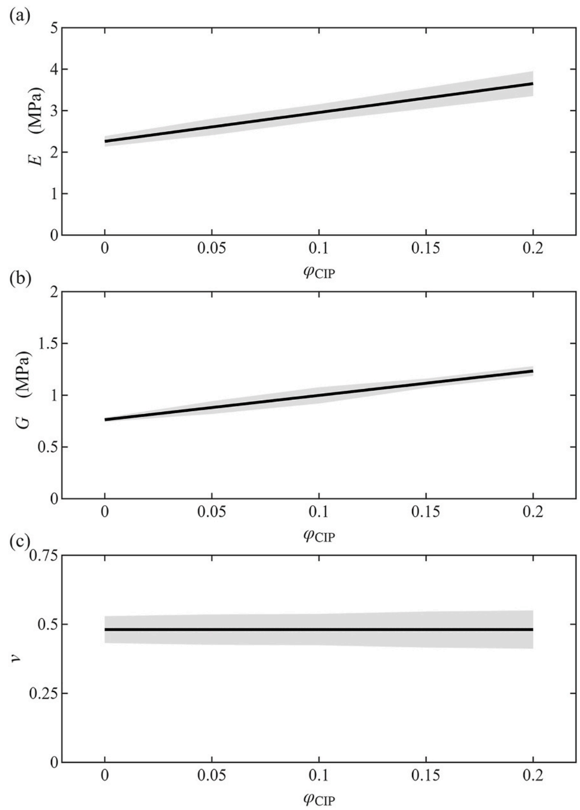

Fig. 9. Estimated elastic properties of the composite as functions of filler volume fraction. The solid line represents the model prediction while the grey shaded region represents the RRMSE associated with each particle volume fraction. (a) Elastic modulus, (b) shear modulus and (c) Poisson's ratio.

$$\Delta M = 100 \cdot \frac{|M(S,\varphi) - M(S=0,\varphi)|}{M(S=0,\varphi)} \tag{21}$$

Fig. 10 summarizes the resulting analysis. In Fig. 10 (a), Eq. (21) is represented as a function of shape factor for $M = \{E, G, \nu\}$. The different line styles correspond to each property, while the colors represent the limiting particle volume fractions (0 % and 20 %). The horizontal line indicates the selected 10 % admissibility threshold. In Fig. 10 (b), the boundaries of constant deviation $\Delta M = 10$ % are mapped in the (L, d) space. Each line corresponds to a constant shape factor for which the deviation of a given property reaches the prescribed limit. Specimens located below and to the right of these lines exhibit deviations smaller than 10 % and therefore provide measurements that can be considered moderately accurate. The black markers indicate the geometries tested in the present study.

The results reveal a markedly different sensitivity of the effective elastic properties to specimen geometry. The compressive modulus and Poisson's ratio exhibit a steep increase with shape factor, even in the low S regime. For geometries typically employed in standard compression tests, corresponding to $S \approx 0.58$ [18,38], the effective compressive modulus exceeds the material modulus value by approximately 64 %. The influence of particle volume fraction on this behavior is negligible, leading to nearly overlapping curves for 0 % and 20 % in Fig. 10. In contrast, the shear modulus shows a weaker dependence on shape factor and approaches an asymptotic regime at large S. As a result, accurate measurements can still be obtained for relatively large shape factors. For the unfilled material, the 10 % deviation threshold is reached at $S \approx 1.33$, while for the highest particle concentration this limit shifts to $S \approx 2.22$. This dependence reflects the increasing role of filler reinforcement in modulating the geometry-induced bias in torsion measurements.

The representation in Fig. 10 (b) provides a direct guideline for specimen design. The admissible region defined by $\Delta M \leq 10$ % can be translated into combinations of diameter and length, enabling selection of geometries that minimize the influence of the shape factor in the measurement. The comparison with the tested specimens shows that several configurations commonly used in practice lie outside this admissible region, particularly for compression measurements. Consequently, standard specimen geometries may lead to significant overestimation of the elastic modulus, whereas torsion measurements remain comparatively robust over a wider range of geometries, although typical disk-like samples can reach shape factors as high as $S = 5$ [39], for which the obtained effective shear modulus is heavily reduced.

For Poisson's ratio, the admissible limit is reached at significantly lower shape factors ($S \approx 0.11$), which fall outside the range of practically achievable geometries. None of the specimens tested in this work lie within this limit due to both equipment constraints (compression clamps restrict the maximum specimen length to approximately 10 mm) and handling limitations, as a specimen with $L = 10$ mm and $S \leq 0.11$ would require a diameter $d \leq 4.4$ mm. Consequently, determination of Poisson's ratio via indirect methods with errors below 10 % is not feasible using standard compression/torsion based configurations, reinforcing the need for correction methodologies.

7. Conclusions

This work has investigated how specimen geometry has affected the experimental determination of elastic properties in particle-reinforced elastomers using compression and torsion measurements. The measurements have shown that the effective compressive modulus has

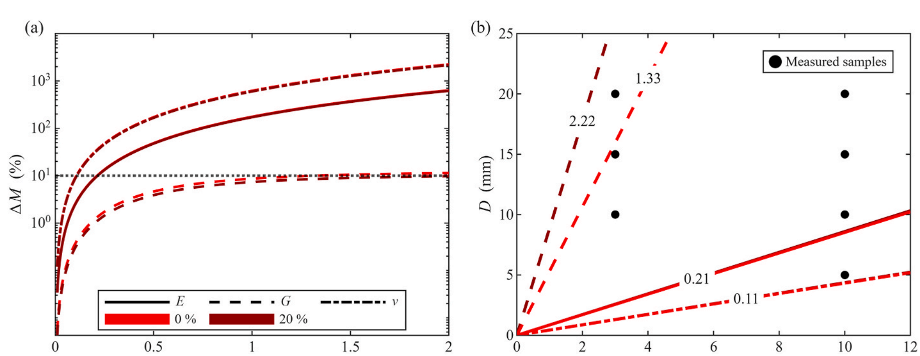

Fig. 10. Quantification of geometry-induced error. (a) Relative deviation as a function of shape factor for the compressive modulus, shear modulus and Poisson's ratio. Different line styles correspond to each property, while colors represent the particle volume fractions. The horizontal dashed line indicates the 10 % admissibility threshold. (b) Mapping of the threshold condition in the (L, d) space. Each line corresponds to a constant shape factor for which the deviation of a given property reaches the prescribed limit. Black markers represent the geometries tested in this work.

increased with shape factor, whereas the effective shear modulus has decreased. In addition, the reinforcement trend obtained directly from the experimental moduli has been found to vary with specimen geometry. These results have demonstrated that properties extracted directly from standard compression and torsion tests have been geometry-dependent effective quantities.

To describe this behavior, a phenomenological model combining filler reinforcement with geometry-dependent relations for compression and torsion has been formulated and identified from the experimental data. This formulation adapts the framework previously developed by the authors for unfilled elastomers to particle-reinforced systems. The model has reproduced the measured effective moduli over the investigated range of particle volume fractions and specimen geometries, with relative root-mean-square errors of approximately 7 % for the compressive modulus, 6 % for the shear modulus and 11 % for Poisson's ratio. The predicted reinforcement slopes have shown that apparent reinforcement has decreased with shape factor in compression and has increased with shape factor in torsion. The results also suggest that particle reinforcement and specimen geometry should not be treated as independent contributions, since the presence of particles modifies the dependence of the effective properties on the shape factor, as reflected by the evolution of the geometry-related parameters with volume fraction.

Within the proposed correction framework, the quasistatic small-strain elastic modulus and shear modulus increase linearly with particle volume fraction. The corresponding Poisson's ratio shows a slight decrease, consistent with the stronger increase of the shear modulus relative to the elastic modulus; however, this variation is lower than the estimated RRMSE and should therefore be interpreted as a weak trend. In addition, a quantitative criterion has been introduced to evaluate the geometry-induced error, defining an admissible region based on a 10 % deviation threshold. The results have shown that standard specimen geometries used in compression testing can lead to significant overestimation of the elastic modulus (e.g., $\approx$64 % for $S \approx 0.58$), whereas shear measurements remain comparatively robust over a wider range of geometries. For Poisson's ratio, the admissible limit is reached at very low shape factors ($S \approx 0.11$), which are not practically achievable under standard testing conditions, preventing its direct determination with comparable accuracy.

Overall, these results provide a model-based framework for estimating geometry-corrected quasistatic small-strain elastic properties of particle-reinforced elastomers from compression and torsion measurements. The proposed approach also provides practical guidelines for specimen design and for the interpretation of geometry-dependent experimental data in small-strain elastic modelling and composite material characterization.

Declaration of generative ai and ai-assisted technologies in the Writing process

During the preparation of this work the authors used ChatGPT-5o to improve the readability and language of the manuscript. After using this tool, the authors reviewed and edited the content as needed and take full responsibility for the content of the published article.

CRediT authorship contribution statement

Julen Cortazar-Noguerol: Conceptualization, Data curation, Formal analysis, Investigation, Methodology, Software, Visualization, Writing – original draft. **Fernando Cortés:** Conceptualization, Formal analysis, Investigation, Methodology, Supervision, Writing – review & editing. **María Jesús Elejabarrieta:** Conceptualization, Formal analysis, Funding acquisition, Investigation, Methodology, Supervision, Writing – review & editing.

Declaration of competing interest

The authors declare that they have no known competing financial interests or personal relationships that could have appeared to influence the work reported in this paper.

Acknowledgements

This research has been supported by the University of Deusto Research Training Grants Program (grant reference number FPI UD_2023_07) and the Department of Education for the Research Group program IT1507-22.

Data availability

Data will be made available on request.

References

[1] R. Ariati, F. Sales, A. Souza, R.A. Lima, J. Ribeiro, Polydimethylsiloxane composites characterization and its applications: a review, Polymers 13 (2021), https://doi.org/10.3390/polym13234258.
[2] S.H. Kwon, J.H. Lee, H.J. Choi, Magnetic particle filled elastomeric hybrid composites and their magnetorheological response, Materials 11 (2018), https://doi.org/10.3390/ma11061040.
[3] W. Xian, Y.-S. Zhan, A. Maiti, A.P. Saab, Y. Li, Filled elastomers: mechanistic and physics-driven modeling and applications as smart materials, Polymers 16 (2024) 1387, https://doi.org/10.3390/polym16101387.
[4] H. Koruk, S. Rajagopal, A comprehensive review on the viscoelastic parameters used for engineering materials, including soft materials, and the relationships between different damping parameters, Sensors 24 (2024) 6137, https://doi.org/10.3390/s24186137.
[5] I.M. Daniel, O. Ishai, I.M. Daniel, O. Ishai, Engineering Mechanics of Composite Materials, second ed., second ed., Oxford University Press, Oxford, New York, 2005.
[6] R.M. Jones, Mechanics of Composite Materials, second ed., CRC Press, Taylor & Francis Group, Boca Raton London New York, 2021.
[7] Sutrisno J. Ubaidillah, A. Purwanto, S.A. Mazlan, Recent progress on magnetorheological solids: materials, fabrication, testing, and applications, Adv. Eng. Mater. 17 (2015) 563–597, https://doi.org/10.1002/adem.201400258.
[8] R.P. Brown, Physical Testing of Rubber, Springer Netherlands, Dordrecht, 1996, https://doi.org/10.1007/978-94-011-0529-3.
[9] G.J. Gerling, S.C. Hauser, B.R. Soltis, A.K. Bowen, K.D. Fanta, Y. Wang, A standard methodology to characterize the intrinsic material properties of compliant test stimuli, IEEE Trans. Haptic 11 (2018) 498–508, https://doi.org/10.1109/TOH.2018.2825396.
[10] W.S. Lee, K.S. Yeo, A. Andriyana, Y.G. Shee, F.R. Mahamd Adikan, Effect of cyclic compression and curing agent concentration on the stabilization of mechanical properties of PDMS elastomer, Mater. Des. 96 (2016) 470–475, https://doi.org/10.1016/j.matdes.2016.02.049.
[11] S.Z. Qamar, M. Akhtar, T. Pervez, M.S.M. Al-Kharusi, Mechanical and structural behavior of a swelling elastomer under compressive loading, Mater. Des. 45 (2013) 487–496, https://doi.org/10.1016/j.matdes.2012.09.020.
[12] E. Roels, A. Costa Cornellà, J. Brancart, A standardized framework for elastomer characterization in soft robotics, Adv. Intell. Syst. (2025) e202500699, https://doi.org/10.1002/aisy.202500699 n/a.
[13] J.F. Davalos, P. Qiao, J. Wang, H.A. Salim, J. Schlussel, Shear moduli of structural composites from torsion tests, J. Compos. Mater. 36 (2002) 1151–1173, https://doi.org/10.1177/0021998302036010486.
[14] I. Agirre-Olabide, M.J. Elejabarrieta, Maximum attenuation variability of isotropic magnetosensitive elastomers, Polym. Test. 54 (2016) 104–113, https://doi.org/10.1016/j.polymertesting.2016.06.021.
[15] Y. Bai, H. Wei, J. Gu, Z. Zhao, C. Zhang, Size-dependent mechanical behaviors of 3D woven composite under high strain-rate compression loads, Polym. Test. 127 (2023) 108176, https://doi.org/10.1016/j.polymertesting.2023.108176.
[16] J. Cortazar-Noguerol, F. Cortés, I. Agirre-Olabide, M.J. Elejabarrieta, Compression and torsion testing for elastic moduli and Poisson's ratio characterization in silicone rubber samples with varying shape factors, Polym. Test. 149 (2025) 108858, https://doi.org/10.1016/j.polymertesting.2025.108858.
[17] J. Cortazar-Noguerol, F. Cortés, M.J. Elejabarrieta, Influence of the sample shape factor on the dynamic characterization of viscoelastic properties: complex moduli and Poisson's ratio, Eur. J. Mech. ASolids 117 (2026) 105963, https://doi.org/10.1016/j.euromechsol.2025.105963.
[18] ISO 7743:2017 Rubber, Vulcanized or Thermoplastic — Determination of Compression stress-strain Properties. ISO; n.d..
[19] H. Vatandoost, M. Hemmatian, R. Sedaghati, S. Rakheja, Effect of shape factor on compression mode dynamic properties of magnetorheological elastomers, J. Intell. Mater. Syst. Struct. 32 (2021) 1678–1699, https://doi.org/10.1177/1045389X20983921.

[20] A. Yaghoobi, A. Jalali, M. Norouzi, M. Ghatee, Aspect ratio dependency of magneto-rheological elastomers in dynamic tension-compression loading, IEEE Trans. Magn. 58 (2022) 1–13, https://doi.org/10.1109/TMAG.2022.3152031.
[21] D. Borin, N. Kolsch, G. Stepanov, S. Odenbach, On the oscillating shear rheometry of magnetorheological elastomers, Rheol. Acta 57 (2018) 217–227, https://doi.org/10.1007/s00397-018-1071-2.
[22] D. Fauser, J.A. Rodríguez Agudo, H. Madadi, J. Haeberle, J. Renner, H. Steeb, Complex Poisson's ratio for viscoelastic materials: direct and indirect measurement methods and their correlation, Proc. R Soc. Math. Phys. Eng. Sci. 481 (2025), https://doi.org/10.1098/rspa.2024.0543.
[23] G. Heinrich, M. Klüppel, T. Vilgis, Reinforcement of elastomers, Curr. Opin. Solid State Mater. Sci. 6 (2002) 195–203, https://doi.org/10.1016/S1359-0286(02)00030-X.
[24] J. Bergström, M. Boyce, Mechanical behavior of particle filled elastomers, Rubber Chem. Technol. 72 (1999) 633–656, https://doi.org/10.5254/1.3538823.
[25] A.I. Medalia, G. Kraus, Reinforcement of elastomers by particulate fillers. Sci. Technol. Rubber, Academic Press, 1994, pp. 387–418, https://doi.org/10.1016/B978-0-08-051667-7.50013-5.
[26] S.R. Khimi, K.L. Pickering, Comparison of dynamic properties of magnetorheological elastomers with existing antivibration rubbers, Composites, Part B Eng. 83 (2015) 175–183, https://doi.org/10.1016/j.compositesb.2015.08.033.
[27] A. Dargahi, R. Sedaghati, S. Rakheja, On the properties of magnetorheological elastomers in shear mode: design, fabrication and characterization, Composites, Part B Eng. 159 (2019) 269–283, https://doi.org/10.1016/j.compositesb.2018.09.080.
[28] A. Boczkowska, S.F. Awietjan, S. Pietrzko, K.J. Kurzydłowski, Mechanical properties of magnetorheological elastomers under shear deformation, Composites, Part B Eng. 43 (2012) 636–640, https://doi.org/10.1016/j.compositesb.2011.08.026.
[29] D. Garcia-Gonzalez, M.A. Moreno, L. Valencia, A. Arias, D. Velasco, Influence of elastomeric matrix and particle volume fraction on the mechanical response of magneto-active polymers, Composites, Part B Eng. 215 (2021) 108796, https://doi.org/10.1016/j.compositesb.2021.108796.
[30] E. Guth, Theory of filler reinforcement, J. Appl. Phys. 16 (1945) 20–25, https://doi.org/10.1063/1.1707495.
[31] ELASTOSIL® M 4644 A/B | room temperature curing silicone rubber (RTV-2) | Wacker Chemie AG. WACKER Website n.d. https://www.wacker.com/h/en-us/c/elastosil-m-4644-ab/p/000005351 (accessed April 27, 2026)..
[32] Modela MDX-40A 3D milling machine | Roland DGA. Roland Website n.d. https://www.rolanddga.com/es-la/soporte/products/milling/modela-mdx-40a-3d-milling-machine (accessed February 6, 2025).
[33] N.W. Tschoegl, W.G. Knauss, I. Emri, Poisson's Ratio in Linear Viscoelasticity – a Critical Review, 2002.
[34] Mathworks Fmincon Documentation n.d. https://es.mathworks.com/help/optim/ug/fmincon.html (accessed September 22, 2025).
[35] A.A. Filippov, V.M. Fomin, E.V. Karpov, Experimental determination of the elastic characteristics of filled polymers using mechanical tests for constrained compression, Novosibirsk, Russia, https://doi.org/10.1063/1.5117374, 2019.
[36] Y. Xu, M. Li, H. Li, S. Zhang, H. Wang, X. Guo, et al., The study on the mechanical properties of magnetorheological elastomers under triaxial compression, J. Intell. Mater. Syst. Struct. 32 (2021) 1256–1266, https://doi.org/10.1177/1045389X20978279.
[37] L.M. Lektrova, P.V. Melent'ev, YuV. Zelenev, Influence of fillers on the poisson ratios of rubber-like polymers, Polym. Mech. 9 (1975) 308–309, https://doi.org/10.1007/BF00855057.
[38] D11 Committee. Test methods for rubber properties in compression n.d. https://doi.org/10.1520/D0575-91R24..
[39] ISO 3219-2:2022 Rheology - Part 2: General Principles of Rotational and Oscillatory Rheometry. ISO; n.d.